nanomaterials

MDPI

Article

Two-Dimensional Perovskite Crystals Formed by Atomic Layer Deposition of $CaTiO_3$ on γ-Al_2O_3

Tianyu Cao, Ohhun Kwon, Chao Lin, John M. Vohs and Raymond J. Gorte *

Department of Chemical and Biomolecular Engineering, University of Pennsylvania, Philadelphia, PA 19104, USA; caot@seas.upenn.edu (T.C.); ohhun@seas.upenn.edu (O.K.); linchao@seas.upenn.edu (C.L.); vohs@seas.upenn.edu (J.M.V.)
* Correspondence: gorte@seas.upenn.edu

Abstract: $CaTiO_3$ films with an average thickness of 0.5 nm were deposited onto γ-Al_2O_3 by Atomic Layer Deposition (ALD) and then characterized by a range of techniques, including X-ray Diffraction (XRD) and High-Resolution, Transmission Electron Microscopy (HRTEM). The results demonstrate that the films form two-dimensional crystallites over the entire surface. Lattice fringes from HRTEM indicate that the crystallites range in size from 5 to 20 nm and are oriented in various directions. Films of the same thickness on SiO_2 remained amorphous, indicating that the support played a role in forming the crystallites.

Keywords: perovskites; thin films; crystallization; atomic layer deposition

Citation: Cao, T.; Kwon, O.; Lin, C.; Vohs, J.M.; Gorte, R.J. Two-Dimensional Perovskite Crystals Formed by Atomic Layer Deposition of $CaTiO_3$ on γ-Al_2O_3. *Nanomaterials* **2021**, *11*, 2207. https://doi.org/10.3390/nano11092207

Received: 3 August 2021
Accepted: 25 August 2021
Published: 27 August 2021

1. Introduction

Thin oxide films on high-surface-area substrates could be important for a number of applications, including novel heterogeneous catalysts [1] and new materials for chemical looping [2]. The standard impregnation of metal salts can give monolayer oxides when there are favorable interactions with the support, such as in the case of titania-supported vanadia catalysts [3]; however, when the impregnated amount is in excess of a monolayer, three-dimensional particles are usually formed [4]. Recent interest in adding the second oxide by Atomic Layer Deposition (ALD) results from the fact that uniform, two-dimensional layers which are thicker than one monolayer can be formed by this procedure [5–8]. In some applications, the crystallinity of the two-dimensional film could be very important.

An interesting example where thin films are important is that of perovskite-supported metals. These have been referred to as "Intelligent Catalysts" because the reversible ingress and egress of the metal catalyst into the perovskite lattice can potentially be used to redisperse the metal after sintering [9,10]. Strong interactions between the perovskite and the metal can also affect other properties of the metal. For example, Ni supported on Ti-based perovskites have been shown to exhibit extreme tolerance against coking [11] while still showing a high activity for the reforming of methane [12]. However, the implementation of these catalysts has been limited by the low surface areas of typical perovskites and by the fact that much of the metal remains in the perovskite lattice, inaccessible for reactions [1]. Both problems can be solved by having the perovskite in the form of a thin film on a second, high-surface-area oxide. Since the perovskite structure of the oxide is critical for establishing the catalytic properties of Intelligent Catalysts [13], the characterization of the structure of the film is critical.

For a supported thin film to retain a high surface area, the thickness cannot be greater than about 1 nm. This is illustrated by considering that a 1 nm film with a density of 5 g/cm^3 on a 200 m^2/g support would have a mass equal to that of the underlying support. Assuming that the surface area does not decrease even more due to the shrinkage of the pores, the specific surface area would still decrease by a factor of two simply due to the increase in the mass of the sample. However, since the unit cell size of oxides with

perovskite or fluorite structures is only about 0.5 nm, the crystallinity of a 1 nm film would depend on the in-plane ordering of the cations. The characterization of this ordering by techniques like X-ray Diffraction (XRD) is challenging since the film thickness is less than the X-ray coherence length.

Consistent with the films being thinner than the X-ray coherence length, studies from our laboratories of CeO_2 [14], ZrO_2 [15], and $CeZrO_4$ [16] films less than 1 nm in thickness and deposited onto Al_2O_3 by ALD showed these to be X-ray amorphous, even for oxide loadings as high as nearly 40 wt% and calcination temperatures above 1073 K. However, later investigations of mixed oxides with stoichiometries of $LaFeO_3$ [17,18] and $CaTiO_3$ [12,19] reported intense perovskite XRD peaks for even lower loadings on $MgAl_2O_4$ supports, even though other characterization techniques indicated that the films remained intact and did not coalesce into particles. Furthermore, X-ray line broadening of the perovskite features indicated crystallite sizes between 10 and 20 nm [1], which was inconsistent with there being sufficient material to cover the surface of the support. Since diffraction in the direction perpendicular to the plane of a two-dimensional crystallite is possible [20], it was suggested that the films formed flat crystallites with random surface orientations [1]. The direct observation of these crystallites by electron microscopy was difficult however, due to the underlying crystallinity of the $MgAl_2O_4$ support.

In the present study, we investigated $CaTiO_3$ films on a γ-Al_2O_3 support to look for direct evidence of crystallinity in two-dimensional films. In previous research, $CaTiO_3$ film has proven itself a promising support for both noble metal catalysts [19,21] and Ni-based catalysts [12]. γ-Al_2O_3 was chosen as the support because of its relatively poor crystallinity and low reactivity with $CaTiO_3$. Although $CaAl_2O_4$ formation is possible, the spinel structure is easily distinguished from that of a perovskite phase if it should form.

2. Materials and Methods

2.1. Sample Preparation

Fresh γ-Al_2O_3 (Strem Chemicals, Inc., Newburyport, MA, USA, 180 m^2/g) was first calcined in air at 1173 K for 24 h to achieve a stable support with a surface area of 105 m^2/g, and the diameter of the calcined Al_2O_3 particles ranged between 5–30 nm. ALD was performed in a static system that has been described in detail elsewhere [15]. The precursors were $Ca(TMHD)_2$ (TMHD=2,2,6,6-tetramethyl-3,5-heptanedionato, Strem Chemicals, Inc., Newburyport, MA, USA) and $TiCl_4$ (Sigma-Aldrich, St. Louis, MO, USA). For CaO deposition, the sample was exposed to vapors from the Ca precursor for 5 min at 573 K; ligand removal was accomplished by oxidizing the sample in air at 873 K in a muffle oven for 5 min. For TiO_2 deposition, the sample was exposed to $TiCl_4$ vapor at 423 K for 3 min; oxidation was accomplished by exposure to humidified air (containing 10% steam) at 423 K. Growth rates were determined by weighing the sample after every ALD cycle, as shown in Figure S3, and were found to be 6.6×10^{13} Ca atom/cm^2-cycle (equivalent to 0.018 nm of CaO per cycle, assuming a bulk density for the film) and 9.6×10^{13} Ti atom/cm^2-cycle (0.030 nm of TiO_2 per cycle). To achieve the correct perovskite stoichiometry, we performed six ALD cycles of CaO, followed by four cycles of TiO_2. The elemental composition of the deposited sample was further tested by the inductively coupled plasma−optical emission spectrometry (ICP-OES) method on a Spectro Genesis spectrometer equipped with a Mod Lichte nebulizer. Finally, the $CaTiO_3/Al_2O_3$ sample was calcined in air at 1073 K for 3 h. The calculated thickness of the $CaTiO_3$ film was 0.52 nm, determined from the mass of deposited $CaTiO_3$ and the BET surface area of the Al_2O_3, assuming a uniform film with the bulk density of $CaTiO_3$ (3.98 g cm^{-3}) [12].

2.2. Sample Characterization

X-ray Diffraction (XRD) was performed on a Rigaku MiniFlex diffractometer (Rigaku Analytical Devices, Inc., Wilmington, MA, USA) equipped with a Cu K-α source (λ = 0.15406 nm). Scanning transmission electron microscopy (STEM) and high-resolution transmission electron microscopy (HR-TEM) images and Energy Dispersive X-ray Spectra

(EDS) were acquired on a JEOL JEM-F200 STEM (JEOL USA Inc., Peabody, MA, USA), operated at 200 kV. For the TEM analysis, the sample was ground with a mortar and pestle and then dispersed in ethanol to form a suspension. A single drop of the suspension was then added to a standard TEM sample grid (Ted Pella, Inc., Redding, CA, USA), which was then allowed to dry. Temperature Programmed Desorption (TPD) measurements were performed in high vacuum using equipment that is described in detail elsewhere [22]. During the TPD experiment, the samples were first exposed to 2-propanol vapor at room temperature, then evacuated for 1 h using a turbo-molecular pump. The sample temperature was then ramped at 10 K min^{-1} while monitoring the desorbing species using a quadrupole mass spectrometer (SRS-RGA-100, Stanford Research Systems, Sunnyvale, CA, USA).

3. Results

The XRD patterns of the 18 wt% $CaTiO_3/Al_2O_3$ sample and the bare Al_2O_3 support are presented in Figure 1. The pattern for bare Al_2O_3 shows weak, broad peaks, consistent with a low degree of crystallinity, while the $CaTiO_3$-containing sample shows additional features at 23, 33, 48, 59 degrees 2θ that can be assigned to the $CaTiO_3$ perovskite phase, even though the thickness of the film (0.52 nm) was much smaller than the coherence length of XRD. Based on the linewidth of the feature at ~33 degrees, the crystallite size of the perovskite phase is estimated to be ~17 nm. The two small peaks at 25 and 27 degrees can be assigned to the (101) peak of an anatase phase and the (110) peak of a rutile phase. Both peaks are the strongest features of their respective phases and suggest that there was a slight excess of TiO_2 in the sample. The ICP-OES results showed that the weight loading of $CaTiO_3$ on Al_2O_3 was 16.7 wt%, consistent with that acquired by weight tracking. The ratio between Ca and Ti was 0.95:1 and agreed with the XRD results. It is worth noting that if all of the perovskite phase were present as three-dimensional particles, 17 nm in size, the amount of $CaTiO_3$ in the sample would be sufficient to cover only a very small fraction of the Al_2O_3.

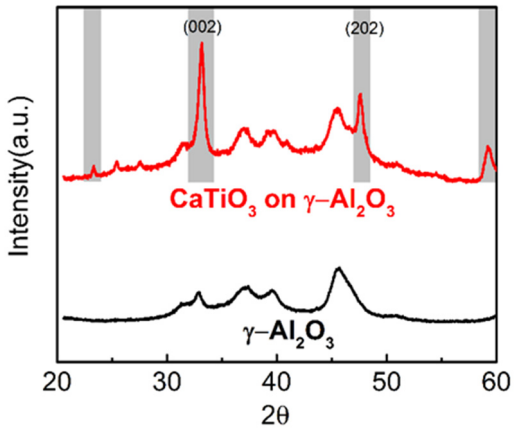

Figure 1. XRD patterns of bare Al_2O_3 (γ-phase, denoted as the black line) and the 18 wt% $CaTiO_3/Al2O_3$ sample (denoted as the red line). Features shaded in grey correspond to peaks of the perovskite phase.

To determine the morphology of the added $CaTiO_3$, Scanning Transmission Electron Microscope (STEM) images with Energy Dispersive X-ray Spectra (EDS) were obtained, as shown in Figure 2a–d. The STEM images of $CaTiO_3/Al_2O_3$ were indistinguishable from those of Al_2O_3. The EDS maps of Ca, Ti and Al were more informative and show uniform distributions of Ca and Ti over the entire surface.

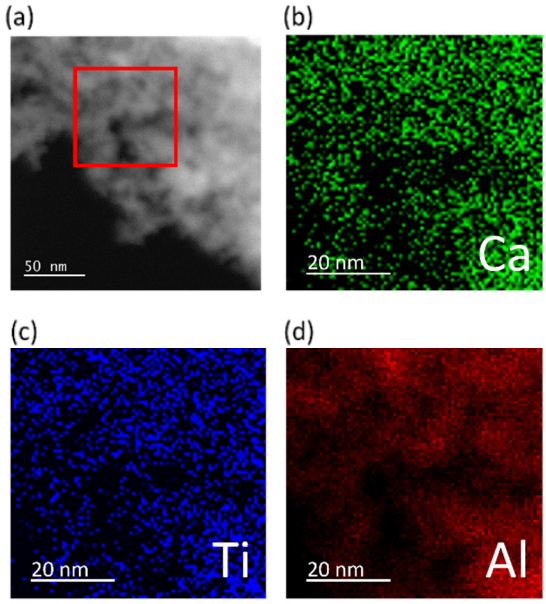

Figure 2. (**a**) High angle annular dark field (HAADF) STEM image of the 18 wt% $CaTiO_3/Al_2O_3$ sample; (**b**–**d**) are EDS maps of Ca, Ti and Al, taken from the region indicated by the red frame.

Further evidence for the $CaTiO_3$ forming a uniform film comes from Temperature Programmed Desorption (TPD) measurements reported in Figure 3. Al_2O_3 is a Lewis acid and is a good catalyst for alcohol dehydration. As discussed in more detail elsewhere [23], room-temperature exposure of Al_2O_3 to 2-propanol, followed by evacuation, leaves approximately one monolayer of the alcohol on the surface. As shown by the TPD in Figure 3a, about half of this adsorbed alcohol leaves the surface as 2-propanol (m/e = 45, 43, and 41) below 400 K, with the rest reacting to propene (m/e = 41) and water, with propene desorbing between 400 and 500 K. The analogous results for the 18 wt% $CaTiO_3/Al_2O_3$ sample are presented in Figure 3b. Significant amounts of unreacted 2-propanol again desorbed from the sample below 400 K. However, we also observed acetone (m/e = 43) and propene from 575 K to 700 K. For the present purposes, it is noteworthy that desorption features associated with the bare Al_2O_3 are completely absent. If a significant fraction of the Al_2O_3 remained uncovered, one would have observed a propene feature in the TPD below 500 K.

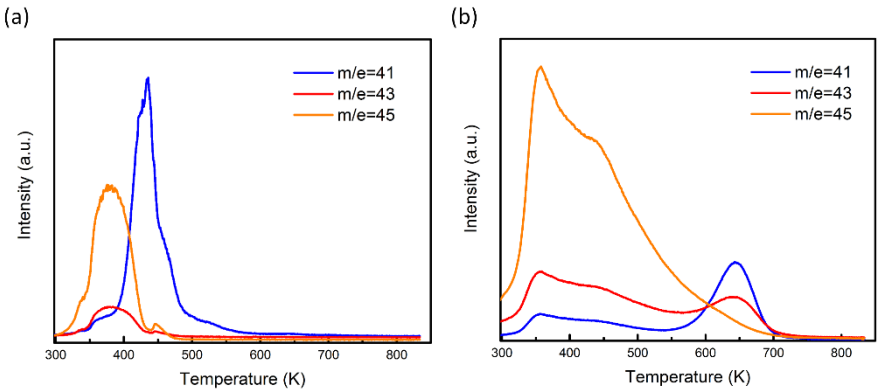

Figure 3. TPD of 2-propanol from (**a**) bare Al_2O_3; (**b**) Al_2O_3 loaded with 18 wt% $CaTiO_3$. Desorption features correspond to propene (m/e = 41), acetone (m/e = 43), and unreacted 2-propanol (m/e = 41, 43, and 45).

While the XRD pattern suggested that the $CaTiO_3$ was present in the form of ~17 nm crystallites, the STEM results in Figure 2 and the TPD results in Figure 3 demonstrated that

the $CaTiO_3$ must be present as a uniform film no more than ~0.5 nm in thickness. However, if even a fraction of the 17 nm crystallites were three-dimensional, there would be insufficient material to completely cover the Al_2O_3 support. This is shown diagrammatically in Figure 4, in which Figure 4a demonstrates the pristine state of the Al_2O_3 support. If the crystallized $CaTiO_3$ were present as three-dimensional, cubic crystallites with an edge length of 10 nm shown in Figure 4c, then 18 wt% $CaTiO_3$ would be sufficient to occupy only 5% of the 105 m^2/g Al_2O_3. Both the STEM/EDS and 2-propanol TPD results imply that the morphology of the film must be more similar to that shown in Figure 4b.

The crystallinity of the $CaTiO_3$ films was further assessed by High Resolution Transmission Electron Microscopy (HR-TEM), with representative images of the bare and $CaTiO_3$-covered Al_2O_3 reported in Figure 5. The image of Al_2O_3 in Figure 5a does not exhibit any well-defined lattice fringes, consistent with the broad peaks found in the XRD pattern of Figure 1. By contrast, the entire surface of the $CaTiO_3/Al_2O_3$ sample, shown in Figure 5b, is covered with lattice fringes. Distinguishable crystallites in Figure 5b are framed by the dashed red lines. Most of the crystallites seem to be between 5 and 10 nm in size, with some of the fringes extending over significantly larger dimensions.

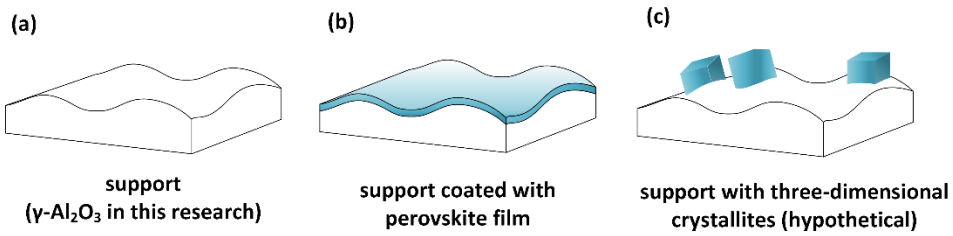

Figure 4. Morphology of the $CaTiO_3$ film on the surface of the Al_2O_3 support. (**a**) Bare support; (**b**) support coated with a uniform film; (**c**) support decorated with three-dimensional cubic crystallites.

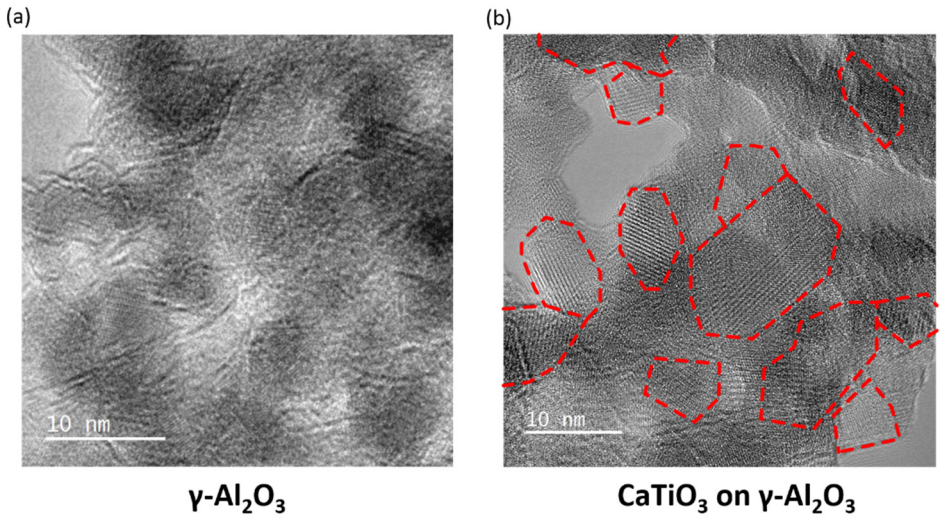

Figure 5. HR-TEM image of (**a**) bare Al_2O_3; (**b**) 18 wt% $CaTiO_3/Al_2O_3$.

In the HR-TEM image of the $CaTiO_3/Al_2O_3$ sample in Figure 6, we focused on regions of the sample that exhibited better crystallization in order to index some of the observed planes. As shown in yellow, fringes could be easily identified with d-spacing corresponding to (002) planes, consistent with these being the most intense feature in the XRD patterns presented in Figure 1. At least one of these crystallites appears to be greater than 20 nm in size (denoted as the red-framed region in Figure 6), consistent with the crystallite-size estimates from XRD. Lattice spacings corresponding to the (202) planes were observed in other images, as shown in Figure S1 (The lattice parameters as well as the d-spacing values for bulk $CaTiO_3$ are presented in Table S1).

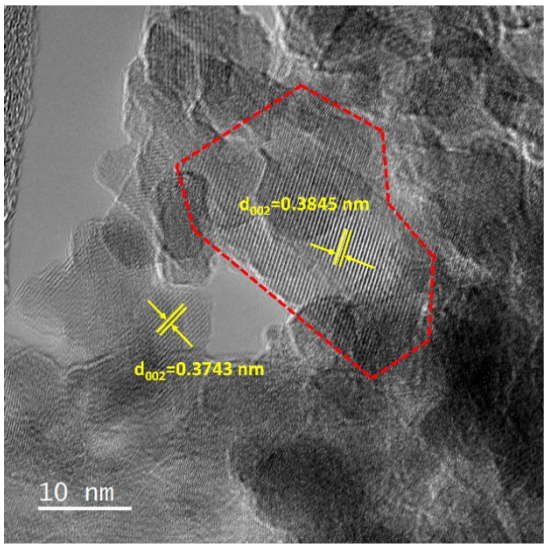

Figure 6. HR-TEM image of the 18 wt% $CaTiO_3/Al_2O_3$ sample.

The question arises whether the Al_2O_3 support plays a role in crystallizing the perovskite film. To address this issue, we also deposited a 0.5 nm film (0.37 g/g SiO_2) of a mixed oxide with the $CaTiO_3$ stoichiometry (The Ca:Ti ratio of the sample was 0.93:1 based on the ICP-OES results) onto an amorphous silica that had a surface area of 180 m^2/g. Growth rates of CaO and TiO_2 on SiO_2 are presented in Figure S4. The sample was again oxidized at 1073 K for 3 h. As shown in Figure S2, the film was largely amorphous, except for a few minor peaks corresponding to an anatase phase (TiO_2). The absence of diffraction peaks showed conclusively that three-dimensional particles were not formed and that the film was also not crystalline on the length scale of the X-ray. This result is similar to what was observed in earlier attempts to prepare $LaFeO_3$ films on silica, which also failed to find evidence of a perovskite phase from diffraction measurements [24].

4. Discussion

It is interesting to ask why the results on SiO_2 are so different from those on Al_2O_3 and $MgAl_2O_4$ [21,25]. Clearly, the perovskite films are not epitaxially matched to the crystal structures of Al_2O_3 (cubic, a = 0.7912 nm) or $MgAl_2O_4$ (cubic, a = 0.8081 nm) [12]. However, it appears that both Al_2O_3 and $MgAl_2O_4$ are able to nucleate the formation of larger, two-dimensional crystallites while SiO_2 is not. Because the crystallization of a perovskite thin film is a nucleation-controlled process, understanding the manner of nucleation is important. Given the thickness of the thin film in the present research (~0.5 nm), the perovskite film must have crystallized in a "heterogeneous nucleation" manner, during which the "seeding effect" played a major role [26]. The nanoscale seeds at the interface between the overlayer and its support presumably reduce the energy barrier for forming crystallites by promoting nucleation at a specific surface site, thus lowering the temperature required to crystallize the perovskite phase. Seeds that were previously reported to facilitate nucleation are crystallized materials, such as perovskite [27] or an intermetal [28]. In the present study, surface crystallites of Al_2O_3 likely served as the seeds in the nucleation of $CaTiO_3$. By contrast, the crystallization of a perovskite phase on the surface of SiO_2 is more difficult due to a scarcity of nucleation sites. A better understanding of the crystallization process could be achieved with theoretical tools such as the density function theory (DFT).

The diffraction pattern for $CaTiO_3/Al_2O_3$ exhibits the typical powder-pattern behavior, and a better understanding of the nucleation process may provide an opportunity to prepare materials in which certain crystal planes are preferred.

5. Conclusions

We demonstrated that relatively large, two-dimensional perovskite platelets were formed when $CaTiO_3$ films were deposited onto γ-Al_2O_3 by ALD. The Al_2O_3 support facilitated the crystallization of its perovskite overlayer by providing sites for nucleation. The formation of $CaTiO_3$ crystallites on the amorphous SiO_2 support, however, is more difficult.

Supplementary Materials: The following are available online at https://www.mdpi.com/article/10.3390/nano11092207/s1, Figure S1: (a) High angle annular dark field (HAADF) STEM image of the 18-wt% $CaTiO_3/Al_2O_3$ sample; (b–d) are EDS maps of Ca, Ti and Al, taken from the region indicated by the dashed red frame; (e) HR-TEM of the sample, image acquired from the orange framed region, Figure S2: XRD patterns of $CaTiO_3$ deposited on SiO_2, the black line denotes bare SiO_2 and the red line denotes $CaTiO_3/SiO_2$, Figure S3: Growth rate of CaO, TiO_2 on γ-Al_2O_3 as a function of ALD cycles. (a) CaO; (b) TiO_2, Figure S4: Growth rate of CaO, TiO_2 on SiO_2 as a function of ALD cycles. (a) CaO; (b) TiO_2, Table S1: Lattice perimeters and d-spacing values of standard $CaTiO_3$ crystal system.

Author Contributions: Conceptualization, investigation and writing the original draft, T.C.; S/TEM experiments, O.K.; Sample preparation, C.L., T.C.; supervision, reviewing and editing, J.M.V. and R.J.G. All authors have read and agreed to the published version of the manuscript.

Funding: This work was supported by the Air Force Office of Scientific Research, under AFOSR Award No. FA9550-19-1-0326. Some of this work was carried out at the Singh Center for Nanotechnology, part of the National Nanotechnology Coordinated Infrastructure Program, which is supported by the National Science Foundation grant NNCI- 2025608.

Data Availability Statement: The data presented in this study are available upon request from the corresponding author.

Conflicts of Interest: The authors declare no conflict of interest.

References

1. Mao, X.; Lin, C.; Graham, G.W.; Gorte, R.J. A Perspective on Thin-Film Perovskites as Supports for Metal Catalysts. *ACS Catal.* **2020**, *10*, 8840–8849. [CrossRef]
2. Scheffe, J.R.; Allendorf, M.D.; Coker, E.N.; Jacobs, B.W.; McDaniel, A.H.; Weimer, A.W. Hydrogen production via chemical looping redox cycles using atomic layer deposition-synthesized iron oxide and cobalt ferrites. *Chem. Mater.* **2011**, *23*, 2030–2038. [CrossRef]
3. Deo, G.; Wachs, I.E. Predicting molecular structures of surface metal oxide species on oxide supports under ambient conditions. *J. Phys. Chem.* **1991**, *95*, 5889–5895. [CrossRef]
4. Su, S.C.; Bell, A.T. A study of the structure of vanadium oxide dispersed on zirconia. *J. Phys. Chem. B* **1998**, *102*, 7000–7007. [CrossRef]
5. Canlas, C.P.; Lu, J.; Ray, N.A.; Grosso-Giordano, N.A.; Lee, S.; Elam, J.W.; Winans, R.E.; Van Duyne, R.P.; Stair, P.C.; Notestein, J.M. Shape-selective sieving layers on an oxide catalyst surface. *Nat. Chem.* **2012**, *4*, 1030–1036. [CrossRef]
6. O'Neill, B.J.; Jackson, D.H.; Lee, J.; Canlas, C.; Stair, P.C.; Marshall, C.L.; Elam, J.W.; Kuech, T.F.; Dumesic, J.A.; Huber, G.W. Catalyst design with atomic layer deposition. *ACS Catal.* **2015**, *5*, 1804–1825. [CrossRef]
7. Jackson, D.H.; Kuech, T.F. Electrochemical effects of annealing on atomic layer deposited Al_2O_3 coatings on $LiNi_{0.5}Mn_{0.3}Co_{0.2}O_2$. *J. Power Sources* **2017**, *365*, 61–67. [CrossRef]
8. Singh, J.A.; Yang, N.; Bent, S.F. Nanoengineering heterogeneous catalysts by atomic layer deposition. *Annu. Rev. Chem. Biomol. Eng.* **2017**, *8*, 41–62. [CrossRef]
9. Nishihata, Y.; Mizuki, J.; Akao, T.; Tanaka, H.; Uenishi, M.; Kimura, M.; Okamoto, T.; Hamada, N. Self-regeneration of a Pd-perovskite catalyst for automotive emissions control. *Nature* **2002**, *418*, 164–167. [CrossRef]
10. Tanaka, H.; Tan, I.; Uenishi, M.; Kimura, M.; Dohmae, K. Regeneration of palladium subsequent to solid solution and segregation in a perovskite catalyst: An intelligent catalyst. *Top. Catal.* **2001**, *16*, 63–70. [CrossRef]
11. Neagu, D.; Oh, T.-S.; Miller, D.N.; Ménard, H.; Bukhari, S.M.; Gamble, S.R.; Gorte, R.J.; Vohs, J.M.; Irvine, J.T. Nano-socketed nickel particles with enhanced coking resistance grown in situ by redox exsolution. *Nat. Commun.* **2015**, *6*, 9120. [CrossRef]
12. Lin, C.; Jang, J.B.; Zhang, L.; Stach, E.A.; Gorte, R.J. Improved Coking Resistance of "Intelligent" Ni Catalysts Prepared by Atomic Layer Deposition. *ACS Catal.* **2018**, *8*, 7679–7687. [CrossRef]
13. Mao, X.; Foucher, A.C.; Stach, E.A.; Gorte, R.J. "Intelligent" Pt Catalysts Based on Thin $LaCoO_3$ Films Prepared by Atomic Layer Deposition. *Inorganics* **2019**, *7*, 113. [CrossRef]
14. Onn, T.M.; Zhang, S.; Arroyo-Ramirez, L.; Xia, Y.; Wang, C.; Pan, X.; Graham, G.W.; Gorte, R.J. High-surface-area ceria prepared by ALD on Al_2O_3 support. *Appl. Catal. B Environ.* **2017**, *201*, 430–437. [CrossRef]

15. Onn, T.M.; Zhang, S.; Arroyo-Ramirez, L.; Chung, Y.-C.; Graham, G.W.; Pan, X.; Gorte, R.J. Improved thermal stability and methane-oxidation activity of Pd/Al_2O_3 catalysts by atomic layer deposition of ZrO_2. *ACS Catal.* **2015**, *5*, 5696–5701. [CrossRef]
16. Onn, T.M.; Dai, S.; Chen, J.; Pan, X.; Graham, G.W.; Gorte, R.J. High-Surface Area Ceria-Zirconia Films Prepared by Atomic Layer Deposition. *Catal. Lett.* **2017**, *147*, 1464–1470. [CrossRef]
17. Mao, X.; Foucher, A.C.; Montini, T.; Stach, E.A.; Fornasiero, P.; Gorte, R.J. Epitaxial and Strong Support Interactions between Pt and $LaFeO_3$ Films Stabilize Pt Dispersion. *J. Am. Chem. Soc.* **2020**, *142*, 10373–10382. [CrossRef]
18. Mao, X.; Foucher, A.C.; Stach, E.A.; Gorte, R.J. Changes in Ni-NiO equilibrium due to $LaFeO_3$ and the effect on dry reforming of CH_4. *J. Catal.* **2020**, *381*, 561–569. [CrossRef]
19. Lin, C.; Foucher, A.C.; Ji, Y.; Curran, C.D.; Stach, E.A.; McIntosh, S.; Gorte, R.J. "Intelligent" Pt Catalysts Studied on High-Surface-Area $CaTiO_3$ Films. *ACS Catal.* **2019**, *9*, 7318–7327. [CrossRef]
20. Holder, C.F.; Schaak, R.E. Tutorial on Powder X-ray Diffraction for Characterizing Nanoscale Materials. *ACS Nano* **2019**, *13*, 7359–7365. [CrossRef] [PubMed]
21. Lin, C.; Foucher, A.; Ji, Y.; Stach, E.A.; Gorte, R.J. Investigation of Rh-titanate ($ATiO_3$) interactions on high-surface-area perovskites thin films prepared by atomic layer deposition. *J. Mater. Chem. A* **2020**, *8*, 16973–16984. [CrossRef]
22. Cao, T.; Huang, R.; Gorte, R.J.; Vohs, J.M. Endothermic reactions of 1-propanamine on a zirconia catalyst. *Appl. Catal. A Gen.* **2020**, *590*, 117372. [CrossRef]
23. Roy, S.; Mpourmpakis, G.; Hong, D.-Y.; Vlachos, D.G.; Bhan, A.; Gorte, R. Mechanistic study of alcohol dehydration on γ-Al_2O_3. *ACS Catal.* **2012**, *2*, 1846–1853. [CrossRef]
24. Cao, T.; Kwon, O.; Vohs, J.M.; Gorte, R.J. $LaFeO_3$ films on SiO_2 for supported-Pt catalysts. *Int. J. Green Energy* **2021**, 1–9. [CrossRef]
25. Lin, C.; Foucher, A.C.; Stach, E.A.; Gorte, R.J. A Thermodynamic Investigation of Ni on Thin-Film Titanates ($ATiO_3$). *Inorganics* **2020**, *8*, 69. [CrossRef]
26. Bretos, I.; Jimenez, R.; Ricote, J.; Calzada, M.L. Low-temperature crystallization of solution-derived metal oxide thin films assisted by chemical processes. *Chem. Soc. Rev.* **2018**, *47*, 291–308. [CrossRef]
27. Kwok, C.K.; Desu, S.B. Low temperature perovskite formation of lead zirconate titanate thin films by a seeding process. *J. Mater. Res.* **1993**, *8*, 339–344. [CrossRef]
28. Huang, Z.; Zhang, Q.; Whatmore, R. The role of an intermetallic phase on the crystallisation of sol-gel prepared lead zirconate titanate thin films. In Proceedings of the ISAF 1998, Eleventh IEEE International Symposium on Applications of Ferroelectrics (Cat. No. 98CH36245), Montreux, Switzerland, 24–27 August 1998; pp. 151–154.